Intermediate-energy Coulomb excitation of ^{52}Fe

K. L. Yurkewicz,[1,2] D. Bazin,[1] B. A. Brown,[1,2] C. M. Campbell,[1,2] J. A. Church,[1,2,*] D.-C. Dinca,[1,2] A. Gade,[1] T. Glasmacher,[1,2] M. Honma,[3] T. Mizusaki,[4] W. F. Mueller,[1] H. Olliver,[1,2] T. Otsuka,[5,6] L. A. Riley,[7] and J. R. Terry[1,2]

[1]*National Superconducting Cyclotron Laboratory, Michigan State University, East Lansing, Michigan 48824, USA*

[2]*Department of Physics and Astronomy, Michigan State University, East Lansing, Michigan 48824, USA*

[3]*Center for Mathematical Sciences, University of Aizu, Tsuruga, Ikki-machi, Aizu-Wakamatsu, Fukushima 965-8580, Japan*

[4]*Institute of Natural Sciences, Senshu University, Higashimita, Tama, Kawasaki, Kanagawa 214-8580, Japan*

[5]*Department of Physics and Center for Nuclear Study, University of Tokyo, Hongo, Tokyo 113-0033, Japan*

[6]*RIKEN, Hirosawa, Wako-shi, Saitama 351-0198, Japan*

[7]*Department of Physics and Astronomy, Ursinus College, Collegeville, Pennsylvania 19426, USA*

(Received 9 February 2004; published 3 September 2004)

The nucleus ^{52}Fe with ($N=Z=26$) has been investigated using intermediate-energy Coulomb excitation in inverse kinematics. A reduced transition probability of $B(E2;0_1^+\rightarrow 2_1^+)=817(102)\ e^2\ \mathrm{fm}^4$ to the first excited 2^+ state at 849.0(5) keV was deduced. The increase in excitation strength $B(E2\uparrow)$ with respect to the even-mass neighbor ^{54}Fe **(**$B(E2\uparrow)=620(50)\ e^2\ \mathrm{fm}^4$**)** agrees with shell-model expectations as the magic number $N=28$ is approached. This measurement completes the systematics of reduced transition strengths to the first excited 2^+ state for the even-even $N=Z$ nuclei up to mass $A=56$.

DOI: 10.1103/PhysRevC.70.034301 PACS number(s): 27.40.+z, 25.70.De, 23.20.Lv, 23.20.Js

The exotic, self-conjugate nucleus ^{52}Fe has been studied via the method of intermediate-energy Coulomb excitation in inverse kinematics [1–4]. An unexpectedly large value for the reduced transition probability $B(E2;0_1^+\rightarrow 2_1^+)$ in ^{56}Ni [5,6], a key signature of collectivity, places high importance on measurements in the neighborhood of this doubly-magic nucleus. The measurement of the reduced transition probability to the first excited state of ^{52}Fe allows the evolution of the quadrupole collectivity in the chain of Fe isotopes to be tracked across the semi-magic nucleus ^{54}Fe. The ^{52}Fe result also completes the systematics of $B(E2\uparrow)$ values for $N=Z$ nuclei up to mass $A=56$. Experimental interest in the nuclear structure of medium-mass $N=Z$ nuclei has increased as advances in radioactive beam technology have made such nuclei accessible for a greater range of studies. Enhanced neutron-proton correlations in such nuclei, where the neutrons and protons occupy identical orbits, are expected to affect the structure of $N=Z$ nuclei. The manifestation and experimental signatures of these effects are currently under discussion [7,8].

The experiment on ^{52}Fe was performed at the Coupled Cyclotron Facility [9] of the National Superconducting Cyclotron Laboratory at Michigan State University. The ^{58}Ni primary beam was accelerated in the K500 and K1200 cyclotrons to an energy of 140 MeV/nucleon. A secondary beam of ^{52}Fe at 65.2 MeV/nucleon was produced by impinging the primary beam on a 376 mg/cm^2 ^{9}Be production target and selecting the isotopes of interest in the large-acceptance A1900 fragment separator [10]. A 238.4 mg/cm^2 Al wedge was used in the A1900 to provide a better separation of the constituents of the multicomponent fragment beam.

The secondary beam was transported to the experimental area, where the Coulomb excitation target of 257.7 mg/cm^2 ^{197}Au was placed at the center of the Segmented Germanium Array (SeGA), consisting of 18 32-fold segmented high-purity germanium detectors [11]. The high-resolution S800 spectrograph [12] was used to identify the scattered ^{52}Fe particles after interaction with the ^{197}Au target and to measure their scattering angles. The mid-target beam energy was 56.9 MeV/nucleon. Since the magnetic spectrograph was operated in dispersion-matched optics mode and due to the limited target size, the A1900 fragment separator had to restrict the momentum spread of the beam to only 0.5% to ensure a beam spot size smaller than the target dimension.

Identification of the fragments of interest was carried out with the focal plane detector system of the spectrograph [13], two plastic scintillator timing detectors along the beam lines, and a parallel-plate avalanche counter located 138 cm before the Coulomb excitation target. The difference in time-of-flight measured between two scintillators before the target ensured a separation of the constituents of the incoming "cocktail beam". The energy loss in the spectrograph's ion chamber correlated with the time-of-flight served to identify the scattered ^{52}Fe after the Coulomb excitation target. Figure 1 shows the particle identification in the spectrograph without gate on the incoming beam.

SeGA was used to detect de-excitation γ rays from the ^{197}Au target and those emitted from inelastically scattered beam particles. The intrinsic energy resolution of the SeGA detectors is approximately 2.5-2.8 keV (0.2%) at 1332 keV. The segmentation of the SeGA detectors provides a determination of the interaction position of a γ ray to within 0.6 cm FWHM. Experimental information from the detector segments was used to Doppler-reconstruct the γ rays emitted in-flight on an event-by-event basis. While nominally SeGA consists of 18 detectors, a total of 13 segmented germanium

*Present address: Lawrence Livermore National Laboratory, Livermore, CA 94550.

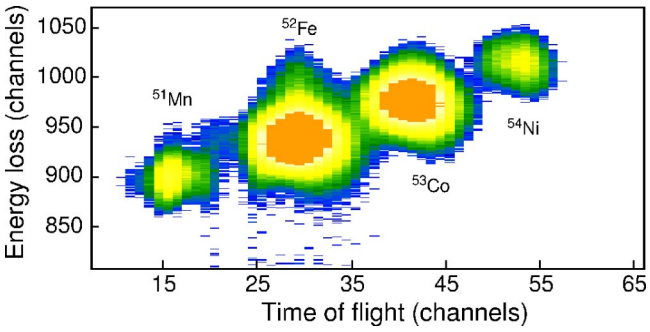

FIG. 1. (Color online) Particle identification of the beam scattered off the Au target. The correlation of the energy loss measured in the ion chamber vs. the time-of-flight resolves the constituents of the "cocktail beam" (1% lower-level cutoff).

detectors were mounted in the array for the present experiment, six detectors in the ring at 37° to the beam direction, and seven in the 90° ring. The set-up of the two rings of SeGA detectors is shown in Fig. 2. The center of the crystal of each detector was at a distance of about 24 cm from the middle of the ^{197}Au target. The energy and efficiency calibrations of the SeGA detectors were carried out with ^{152}Eu and ^{56}Co γ-ray sources covering an energy range from 122 to 3451 keV. The efficiency calibration was performed for each ring of SeGA. The photopeak efficiencies at 849 keV were 1.6(1)% for the 37° ring and 1.1(4)% for the 90° ring, for a sum efficiency of 2.7(2)%.

After the identification of ^{52}Fe nuclei in the S800 focal plane, the coincident γ-ray spectra shown in Fig. 3 were

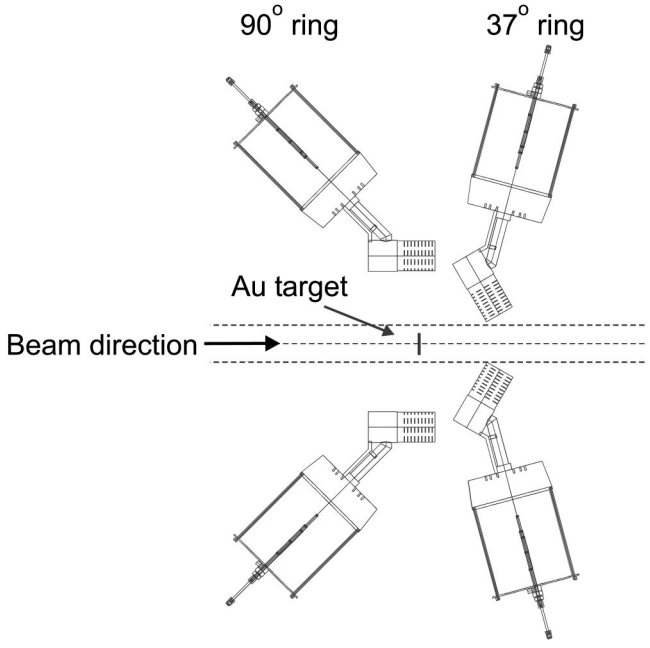

FIG. 2. Schematic set-up of SeGA in the configuration used for Coulomb excitation of ^{52}Fe. The two 37° and 90° rings of SeGA are shown. The angles refer to the directions from the target center to the detector center with respect to the beam direction. A parallel-plate avalanche counter 138 cm upstream of the target position was used to monitor the position of the beam on target.

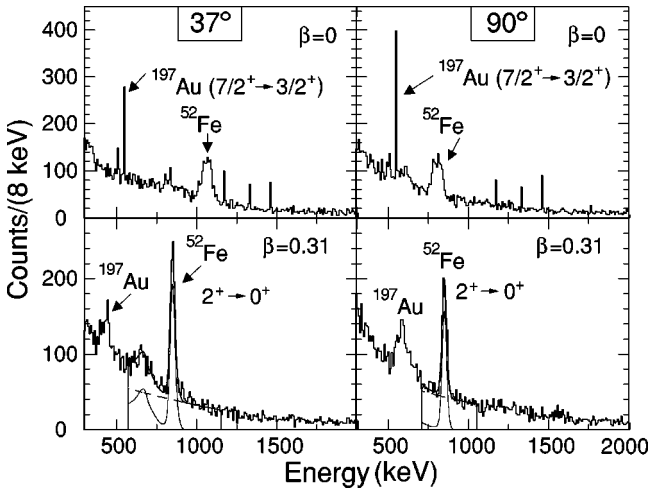

FIG. 3. Gamma-ray spectra in coincidence with ^{52}Fe particles at the S800 focal plane. The transitions corresponding to de-excitation of the ^{197}Au target and ^{52}Fe projectiles are indicated. Laboratory-frame spectra (β=0) are shown in the top panels. Doppler-reconstructed projectile-frame spectra assuming a projectile velocity of β=0.31 at the point of γ-ray emission are shown in the bottom panels with the simulations overlayed. The solid black lines are the total fits to each spectrum, which contain the sum of the simulated response functions (grey lines) and quadratic backgrounds (dashed lines). The γ-ray energies determined as a result of the fits are 849.0(6) and 849.2(8) keV for the 37° and 90° SeGA rings, for a weighted average of 849.1(5) keV.

generated. A strong photopeak at approximately 850 keV is apparent in the projectile-frame spectra shown in the bottom panels of Fig. 3. This γ ray corresponds to the de-excitation from the $J^\pi=2^+$ first excited state to the ground state of ^{52}Fe. In the laboratory-frame spectra (top panels), the 850 keV γ rays become noticeably broader as a result of the angle-dependent Doppler shift to different energies in the 37° ($\approx$1072 keV) and 90° ($\approx$807 keV) rings of SeGA. Since the target and projectile nuclei can both be excited as a result of the inelastic scattering, the 547.5 keV γ ray from the de-excitation of the $J^\pi=7/2^+$ excited state to the $J^\pi=3/2^+$ ground state of the ^{197}Au target nuclei [14] can be seen as a narrow line in the laboratory-frame spectra. In the projectile-frame spectra, the 547 keV γ ray broadens and shifts to approximately 433 keV in the 37° and approximately 575 keV in the 90° ring.

In order to determine the energy and intensity of the γ ray from the de-excitation of ^{52}Fe, a Monte Carlo simulation was performed for ten million incident γ rays at 849 keV, isotropically emitted in the projectile frame and Lorentz boosted with the beam velocity at the time of γ-ray emission. The events were then used by the GEANT [15] code to model the energy deposited in SeGA. These histograms were fit with analytical curves to determine the area under the photopeak, and thus the expected in-beam efficiency. Additionally, simulations for stationary sources were performed and matched with the source calibrations. The simulated efficiency using the GEANT code was scaled upward by 3.5% in the final analysis to reproduce the measured efficiency. The analytical curves were then scaled to fit the experimental spectrum on

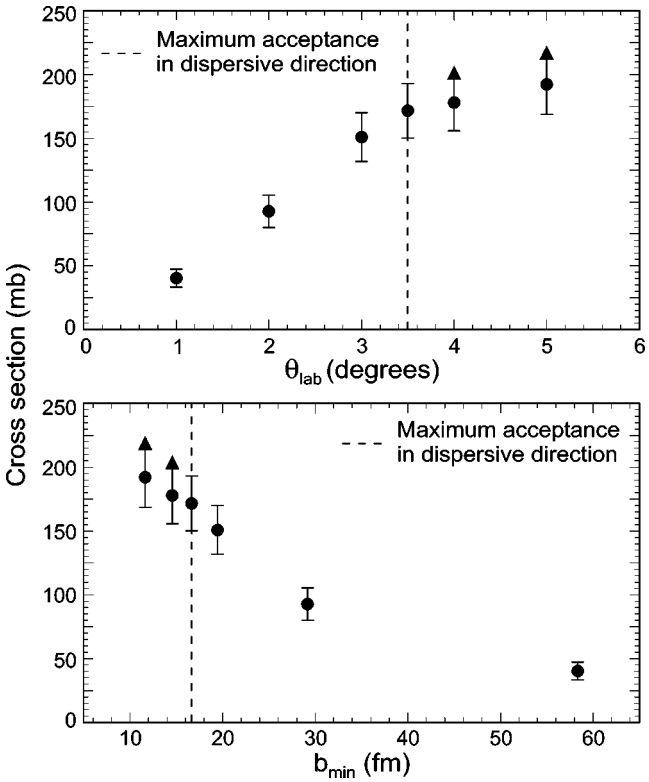

FIG. 4. Measured cross section versus maximum laboratory scattering angle (top) and minimum impact parameter (bottom) for ^{52}Fe nuclei. For each maximum laboratory scattering angle, the corresponding γ-ray spectra and particle spectra were analyzed to yield cross sections. The cross sections measured for 4° and 5° are low due to the loss of acceptance past 3.5° in the dispersive direction, reflected in the lower limits on the error for those cross sections.

top of a quadratic background. The fitting procedure was performed separately for the two SeGA rings. During the fitting process, the amount of scaling was varied but the width and shape of the simulated response functions were fixed. Together with the centroid and area of the simulated photopeak determined from the fit to the simulated spectrum, the scaling of the simulation to the data allowed for a determination of the measured centroid and area of the photopeak observed in the experiment. The bottom panels of Fig. 3 show the fit components and total fit overlayed on the γ-ray spectra detected in coincidence with the scattered ^{52}Fe particles and transformed into the projectile frame. The weighted average of the centroids for the two rings was 849.1(5) keV, in good agreement with the adopted value of E_γ=849.43(10) keV [16] for the de-excitation of the first excited state of ^{52}Fe.

The experimental cross section for Coulomb excitation is given by

$$\sigma = \frac{N_\gamma}{\epsilon_{tot} \times N_{beam} \times N_{target}}. \quad (1)$$

N_γ is the number of detected de-excitation photons, ϵ_{tot} is the total detector photopeak efficiency, N_{beam} is the number of incident secondary beam nuclei, and N_{target} is the number of

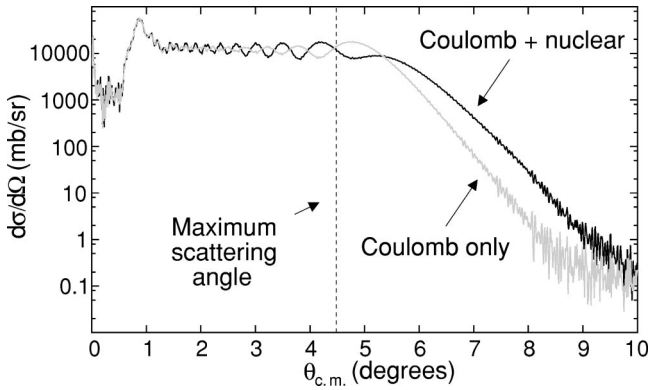

FIG. 5. ECIS calculation for ^{52}Fe at 56.9 MeV/nucleon. Shown are the excitation cross sections as a function of center-of-mass scattering angle for Coulomb excitation only and Coulomb plus nuclear excitation. Parameters from ^{40}Ar scattering on ^{208}Pb at 41 MeV/nucleon were used in the calculation [21]. Below the maximum scattering angle chosen (dashed line), the contribution from nuclear excitations is less than 6%.

target nuclei per unit area. The total efficiency (ϵ_{tot}) includes contributions from the detector efficiency, solid angle covered by the detector array, angular distributions of emitted γ rays due to the Coulomb excitation mechanism and Lorentz boost, and absorption of γ rays in the target material [17].

Events selected to determine the cross section for Coulomb excitation must only include collisions where the minimum impact parameter $b_{\min}$ between the ^{52}Fe and ^{197}Au nuclei exceeds the interaction radius $R_{\rm int}$ to exclude nuclear contributions to the purely electromagnetic Coulomb excitation process. The interaction radius following Wilcke *et al.* [18] is $R_{\rm int}$=13.5 fm for the target-projectile system realized in the present experiment. The interaction in collisions with impact parameters larger than $R_{\rm int}$ is considered to be dominated by the Coulomb force. To calculate the angle-integrated Coulomb excitation cross section (σ) for ^{52}Fe, a maximum laboratory scattering angle of θ_{lab}=3.5°($\theta_{\rm cm}$=4.47°) was chosen. Assuming Coulomb trajectories, this angle corresponds to $b_{\min}$=16.7 fm and a distance of 4.7 fm above the sum of the nuclear radii and exceeding the interaction radius $R_{\rm int}$ by more than 3 fm. The laboratory scattering angle is reconstructed from the magnetic setting of the spectrograph in conjunction with the position information of the nuclei measured in the cathode readout drift chambers of the S800 focal plane. The S800 spectrograph has angle acceptances of ±3.5° in the dispersive direction and ±5° in the nondispersive direction. In order to study the dependence of Coulomb excitation cross section on scattering angle, events were selected with $\theta_{lab}<1°$, 2°, 3°, 3.5°, 4° and 5°. The results are shown in Fig. 4 as a function of maximum laboratory scattering angle and minimum impact parameter. The loss of acceptance beyond 3.5° in the dispersive direction is clearly visible in the upper panel and reflected by the error bars indicating lower limits. A recent intermediate-energy Coulomb excitation experiment on ^{46}Ar also explored the dependence of Coulomb excitation cross section on the impact parameter and it was demonstrated that the $B(E2\uparrow)$ value deduced over a broad range of impact parameters

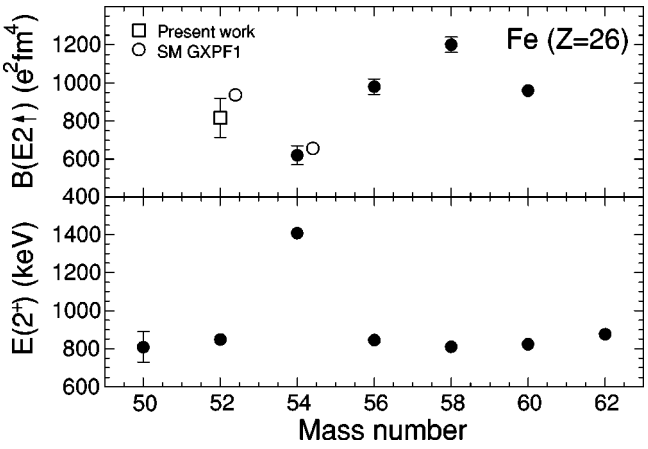

FIG. 6. Systematic behavior of reduced transition probability $B(E2\uparrow)$ and energy of the first excited $J^\pi=2^+$ state $E(2^+)$ for the even-even Fe isotopes. Adopted values, indicated by filled circles, are from [26] while the present measurement is indicated by an open square.

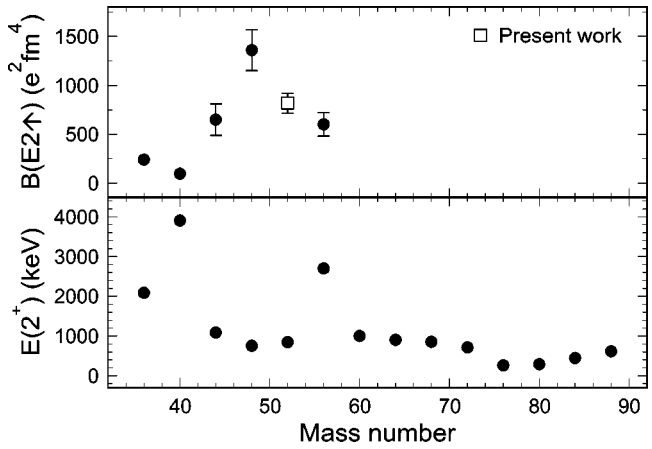

FIG. 7. Reduced transition probability to the first excited $J^\pi=2^+$ state $B(E2\uparrow)$ and energy of the first excited $J^\pi=2^+$ state $E(2^+)$ for the even-even $N=Z$ nuclei with $A\geqslant 36$. The measurement of $B(E2\uparrow)=817(102)\ e^2\mathrm{fm}^4$ for ^{52}Fe is indicated by the open square. Filled circles indicate adopted values, from [26].

(scattering angles) is constant underlining the robustness of this method in the regime of intermediate-energy beams [19].

For events with $\theta_{lab}<3.5°$, the coincident γ-ray spectra were analyzed following the fitting procedure described above to obtain the number of detected γ rays (N_γ). The number of beam particles with the scattering angle restriction was 295 million. With these parameters, a Coulomb excitation cross section to the 849 keV $J^\pi=2^+$ state in ^{52}Fe of $\sigma=172(21)$ mb was extracted.

The uncertainty on the angle-integrated cross section σ includes contributions from the statistical error on N_γ (2.4%) and N_{beam} (<1%), uncertainty on the measurement of the ^{197}Au target thickness (<0.5%), and the error on the γ-ray detection efficiency ϵ_{tot} (7.4%). The uncertainty of the reconstructed laboratory-frame scattering angle is 2 mrad FWHM (±0.05°) [13]. An additional error of approximately 3% corresponding to the percentage difference in excitation cross section for $\theta_{lab}^{\max}-0.05°$ and $\theta_{lab}^{\max}+0.05°$ was included.

Using the theory of Winther–Alder relativistic Coulomb excitation [1] the reduced excitation strength $B(E2;0_1^+\rightarrow 2_1^+)=817(102)\ e^2\mathrm{fm}^4$ was determined from the angle-integrated cross section measured in the experiment for given kinematics and at a minimum impact parameter of $b_{\min}=16.7$ fm. This translates into a half-life for the first 2^+ excited state of $T_{1/2}=7.8(10)$ ps.

While events were chosen to assure at least 4.7 fm between the target and projectile radii, possible nuclear contributions to the cross section were investigated. A calculation for the interaction of ^{52}Fe on ^{197}Au with the Coulomb interaction only, and another with both Coulomb and nuclear interactions allowed, was performed using the ECIS88 coupled-channels code [20]. The calculation used optical model parameters from ^{40}Ar scattering on ^{208}Pb at 41 MeV/nucleon [21]. The angular distributions for the excitation cross sections calculated by the ECIS program are shown in Fig. 5. At scattering angles less than the chosen $\theta_{lab}^{\max}$ of 3.5°, a nuclear contribution of 6% to the excitation cross section was estimated.

Two of the signatures of magic even-even nuclei are a small reduced transition probability to the first excited 2^+ state and a large 2_1^+ excitation energy $E(2_1^+)$. The systematics for both $B(E2\uparrow)$ and $E(2_1^+)$ for the even-even isotopes of Fe are displayed in Fig. 6, including the ^{52}Fe data point from the present work. The isotope ^{54}Fe, with 26 protons and 28 neutrons, has the lowest $B(E2\uparrow)$ value of the series of isotopes and the highest excited state energy [26]. As 28 neutrons completes a closed shell, these results are expected. The present measurement of $B(E2\uparrow)=817(102)\ e^2\mathrm{fm}^4$ for ^{52}Fe, higher than the value for ^{54}Fe, is consistent with ^{54}Fe being semi-magic with $N=28$.

Shell-model calculations of reduced transition probabilities to the first excited states of ^{52}Fe and ^{54}Fe were performed with the conventional shell-model code MSHELL [22] using the GXPF1 interaction [23,24]. The transition strengths were calculated as described in [25], with A_p and A_n the proton and neutron strength amplitudes. A truncation of seven particles excited out of the $f_{7/2}$ orbit was chosen for ^{52}Fe and ^{54}Fe. The calculations were performed with two different sets of effective proton and neutron charges e_p and e_n ($e_p+e_n=2e$ for both sets and $e_p-e_n=0.5e$ and $e_p-e_n=0.7e$, respectively). For both sets of effective charges and strength amplitudes $A_p=A_n=15.35$ the theoretical prediction for the $T_z=0$ nucleus ^{52}Fe was $B(E2;0_1^+\rightarrow 2_1^+)=942\ e^2\mathrm{fm}^4$. For ^{54}Fe, with $A_p=14.63$ and $A_n=7.13$ and effective charges $e_p=1.5e$ and $e_n=0.5e$, $B(E2\uparrow)=651\ e^2\mathrm{fm}^4$ was calculated. With $e_p=1.3e$ and $e_n=0.7e$, the result was $B(E2\uparrow)=576\ e^2\mathrm{fm}^4$. The adopted value of $B(E2\uparrow)=620(50)\ e^2\mathrm{fm}^4$ for the first excited state of ^{54}Fe [26] agrees with both calculations, while the experimental value from the present work of $B(E2\uparrow)=817(102)\ e^2\mathrm{fm}^4$ for ^{52}Fe is slightly lower than the theoretical value. Comparison of the ^{52}Fe and ^{54}Fe experimental $B(E2\uparrow)$ values with the theoretical predictions show that the same trend is observed in both experiment and theory. The shell model, however, appears to over-predict the increase of the ^{52}Fe reduced transition probability from that of ^{54}Fe.

Figure 7 shows the systematics for reduced transition

probabilities and energies of the first excited states for the known even-even $N=Z$ nuclei with $A \geqslant 36$. The present measurement of $B(E2\uparrow)=817(102)\,e^2\mathrm{fm}^4$ to the first excited state of ^{52}Fe indicates a decrease in collectivity from ^{48}Cr to ^{56}Ni.

In summary, the absolute $B(E2;0_1^+ \rightarrow 2_1^+)$ strength in ^{52}Fe was determined via intermediate-energy Coulomb excitation. The value of $B(E2\uparrow)=817(102)\,e^2\mathrm{fm}^4$ emphasizes the existence of the semi-magic shell closure at $N=28$ in the chain of Fe isotopes, in contrast to the situation in the Ni isotopes where $N=Z=28$ ^{56}Ni is found to be rather collective [5,24]. Furthermore, this data point completes the $B(E2\uparrow)$ systematics in $N=Z$ nuclei, now established up to ^{56}Ni.

This work was supported by the National Science Foundation under Grant Nos. PHY-9875122, PHY-0070911, PHY-0110253, INT-0089581, and in part by Grant-in-Aid for Specially Promoted Research (13002001) from the MEXT of Japan, and by the joint large-scale nuclear-structure calculation project by RIKEN and CNS.

[1] A. Winther and K. Alder, Nucl. Phys. **A319**, 518 (1979).
[2] T. Motobayashi, Y. Ikeda, Y. Ando, K. Ieki, M. Inoue, N. Iwasa, T. Kikuchi, M. Kurokawa, S. Moriya, S. Ogawa, H. Murakami, S. Shimoura, Y. Yanagisawa, T. Nakamura, Y. Watanabe, M. Ishihara, T. Teranishi, H. Okuno, and R. F. Casten, Phys. Lett. B **346**, 9 (1995).
[3] H. Scheit, T. Glasmacher, B. A. Brown, J. A. Brown, P. D. Cottle, P. G. Hansen, R. Harkewicz, M. Hellström, R. W. Ibbotson, J. K. Jewell, K. W. Kemper, D. J. Morrissey, M. Steiner, P. Thirolf, and M. Thoennessen, Phys. Rev. Lett. **77**, 3967 (1996).
[4] T. Glasmacher, Annu. Rev. Nucl. Part. Sci. **48**, 1 (1998).
[5] G. Kraus, P. Engelhof, C. Fischer, H. Geissel, A. Himmler, F. Nickel, G. Münzenberg, W. Schwab, A. Weiss, J. Friese, A. Gillitzer, H. J. Körner, M. Peter, W. F. Henning, J. P. Schiffer, J. V. Kratz, and B. A. Brown, Phys. Rev. Lett. **73**, 1773 (1994).
[6] Y. Yanagisawa, T. Motobayashi, S. Shimoura, Y. Ando, H. Fujiwara, I. Hisanaga, H. Iwasaki, Y. Iwata, H. Murakami, T. Minemura, T. Nakamura, T. Nishio, M. Notani, H. Sakurai, S. Takeuchi, T. Teranishi, Y. X. Watanabe, and M. Ishihara, in *Coulomb excitation of* ^{56}Ni, edited by B. M. Sherrill, D.J. Morrissey, and C. N. Davids, AIP Conf. Proc. No. 455 (AIP, New York, 1998) p.610.
[7] A. Johnson, Eur. Phys. J. A **13**, 9 (2002).
[8] W. Satula and R. Wyss, Phys. Rev. Lett. **87**, 052504 (2001).
[9] F. Marti, D. Poe, M. Steiner, J. Stetson, and X. Y. Wu, *Proceedings 16th International Conference on Cyclotrons and Their Applications* (East Lansing, Michigan, 2002).
[10] D. J. Morrissey, B. M. Sherrill, M. Steiner, A. Stolz, and I. Wiedenhöver, Nucl. Instrum. Methods Phys. Res. B **204**, 90 (2003).
[11] W. F. Mueller, J. A. Church, T. Glasmacher, D. Gutknecht, G. Hackman, P. G. Hansen, Z. Hu, K. L. Miller, and P. Quirin, Nucl. Instrum. Methods Phys. Res. A **466**, 492 (2001).
[12] D. Bazin, J. A. Caggiano, B. M. Sherrill, J. Yurkon, and A. Zeller, Nucl. Instrum. Methods Phys. Res. B **204**, 629 (2003).
[13] J. Yurkon, D. Bazin, W. Benenson, D. J. Morrissey, B. M. Sherrill, D. Swan, and R. Swanson, Nucl. Instrum. Methods Phys. Res. A **422**, 291 (1999).
[14] C. Zhou, Nucl. Data Sheets **76**, 399 (1995).
[15] GEANT-detector description and simulation tool, version 3.21, Technical Report W5013, CERN (1994).
[16] H. Junde, Nucl. Data Sheets **90**, 1 (2000).
[17] K. L. Miller, Ph.D. thesis, Michigan State University (2003).
[18] W. W. Wilcke, J. R. Birkelund, H. J. Wollersheim, A. D. Hoover, J. R. Huizenga, W. U. Schröder, and L. E. Tubbs, At. Data Nucl. Data Tables **25**, 391 (1980).
[19] A. Gade, D. Bazin, C. M. Campbell, J. A. Church, D.-C. Dinca, J. Enders, T. Glasmacher, Z. Hu, K. W. Kemper, W. F. Mueller, H. Olliver, B. C. Perry, L. A. Riley, B. T. Roeder, B. M. Sherrill, and J. R. Terry, Phys. Rev. C **68**, 014302 (2003).
[20] J. Raynal, Phys. Rev. C **23**, 2571 (1981); J. Raynal, computer program ECIS88, in workshop on applied theory and nuclear model calculation for nuclear technology application (JCTP), Trieste, 1988.
[21] T. Suomijärvi, D. Beaumel, Y. Blumenfeld, Ph. Chomaz, N. Frascaria, J. P. Garron, J. C. Roynette, J. A. Scarpaci, J. Barrette, B. Fernandez, J. Gastebois, and W. Mittig, Nucl. Phys. **A509**, 369 (1990).
[22] T. Mizusaki, RIKEN Accel. Prog. Rep. **33**, 14 (2000).
[23] M. Honma, T. Otsuka, B. A. Brown, and T. Mizusaki, Phys. Rev. C **65**, 061301 (2002).
[24] M. Honma, T. Otsuka, B. A. Brown, and T. Mizusaki, Phys. Rev. C **69**, 034335 (2004).
[25] B. A. Brown and B. H. Wildenthal, Phys. Rev. C **21**, 2107 (1980).
[26] S. Raman, C. W. Nestor, Jr., and P. Tikkanen, At. Data Nucl. Data Tables **78**, 1 (2001).